JOURNAL OF MATERIALS SCIENCE 21 (1986) 2373–2384

Morphology and mechanical properties of melt-spun and conventionally cast aluminium, AlMg and AlSi alloys before and after hot extrusion

M. VAN ROOYEN, P. F. COLIJN, TH. H. DE KEIJSER, E. J. MITTEMEIJER
Laboratory of Metallurgy, Delft University of Technology, Rotterdamseweg 137, 2628 AL Delft, The Netherlands

Rapidly solidified aluminium, AlMg (0 to 16.5 at% Mg) and AlSi (0 to 20.2 at% Si) alloys were produced by melt spinning. The AlMg ribbons were single-phase, whereas the AlSi ribbons were dual-phase. In the ribbons of both alloy systems the fineness of the microstructure increased with increasing alloying element content. The melt-spun ribbons were consolidated by hot extrusion. For comparison, conventionally cast alloys of corresponding compositions were extruded analogously. During the extrusion process in AlMg (16.5 at% Mg) and in the AlSi alloys precipitation occurred. The consolidation of the ribbons was markedly influenced by the oxide layer on the ribbon surfaces: in the AlSi consolidates a more intimate contact between the ribbons was apparent than in the aluminium and AlMg consolidates. In the extrudates of the conventionally cast alloys the grains and second-phase particles were much larger than in the consolidates. The observed dependence on alloy composition of hardness, ultimate tensile strength and elongation at fracture of both consolidated ribbons and extrudates of the conventionally cast alloys are discussed in terms of matrix grain size, solute content of the matrix, amount and size of second-phase particles and recrystallization behaviour. For all compositions of the alloys the Vickers hardness of the as-melt-spun ribbons was higher than that of the consolidated products, owing to recrystallization and precipitation provoked by the hot consolidation process. The ultimate tensile strength as well as the elongation at fracture of both consolidated ribbons and extruded conventionally cast alloys did not differ significantly for AlMg. However, due to a finer microstructure and a stronger inter-ribbon bonding, for AlSi alloys with a high silicon content the rapid solidification processing route did yield a product with significantly improved mechanical properties as compared with the extruded conventionally cast alloys.

1. Introduction

Although there is a strong and global interest in rapidly quenched metals, it has been stated recently [1]: "Unless some way is found of effectively forcing the practical aspects . . . eventually rapid quenching research will die away and its bright promise will be denied". In particular, an investigation into possible applications of rapidly solidified *crystalline* alloys is desired.

This paper deals with metastable crystalline liquid-quenched (melt-spun) AlMg and AlSi alloys before and after compaction by hot extrusion. The morphology and mechanical properties have been studied and compared with those of conventionally cast alloys.

Various strengthening mechanisms can be utilized to improve the mechanical properties of metallic materials [2]. Commonly one distinguishes

(a) work hardening,
(b) strengthening from grain refinement,
(c) solid-solution hardening,
(d) precipitation or age-hardening and
(e) dispersion hardening.

By rapid quenching from the melt, aluminium alloys can be obtained which exhibit, as compared to conventionally cast alloys [3, 4],

(a) decreased grain size,
(b) increased chemical homogeneity,
(c) enhanced supersaturation of alloying elements and vacancies and
(d) retention/appearance of non-equilibrium crystal structures.

Hence, with reference to the strengthening mechanisms mentioned, rapid-solidification technology can be applied to the production of materials with improved mechanical properties. However, rapid quenching unavoidably leads to (half) products which are small in at least one dimension. Consequently, the utilization of liquid-quenched materials requires a consolidation process after solidification. Such a process

0022–2461/86 $03.00 + .12

implies mechanical and/or thermal treatment, which may cause deterioration of initially useful properties of the material.

Hot extrusion is a frequently applied compaction process. Then, in advance, a number of operations can be carried out in succession:

(a) precompaction (to avoid an excessively large extrusion chamber),
(b) degassing (occassionally necessary to prevent development of hydrogen from adsorbed water) and
(c) preheating.

The extrusion process is controlled by many parameters; the most important are

(a) extrusion ratio,
(b) working temperature,
(c) speed of deformation (ram speed) and
(d) frictional conditions at the die and container wall.

A discussion of the pretreatments and the extrusion process itself can be found elsewhere [5, 6].

The behaviour of the oxide layer on the ribbon surfaces during the deformation process is of crucial significance for the quality of the final product. In the case of an ideal consolidation the oxide layers are broken up and the oxide particles are finely dispersed in the compact. This causes a strengthening effect [5]. The degree of dispersion obtained depends on the adherence of the oxide layer to the ribbon surface; too high a bond strength leads to an insufficient breaking-up of the layer. This prevents intimate contact between ribbons and diffusion welding across the boundaries is impeded; a strong anisotropy of the mechanical properties will result.

Hot working accelerates diffusion and recovery/recrystallization processes. These processes affect the structure and mechanical properties of the extrudates.

It is well understood that more complicated multi-component (aluminium-base) alloys may show properties appropriate for special applications (e.g. [7]). However, until now, the rationale for understanding the relation between treatment and properties is generally lacking, and optimization is pursued in an empirical way. In the present research project binary AlMg and AlSi alloys have been chosen as model systems. These alloy systems allow evaluation of the effectiveness of solid-solution strengthening and dispersion strengthening in rapid-solidification processing.

2. Experimental details

2.1. Production and processing of melt-spun ribbons

Melt-spun ribbons (thickness 25 to 50 μm, width about 2 mm, cooling rate about 10^6 K sec^{-1}) were prepared from pure aluminium, AlMg (2.6, 3.2, 5.6, 11.2 and 16.5 at % Mg) and AlSi (1.1, 2.4, 4.6, 7.2, 11.4 and 20.2 at % Si) using aluminium (99.998 wt %), magnesium (99.38 wt %) and silicon (99.99 wt %).

Extrusion was performed at about 675 K for the AlMg alloys and at about 725 K for aluminium and the AlSi alloys, employing a preheating time of about 40 min. The extrusion ratio was 25 and the extrusion speed was about 1 m min^{-1} (when taking into account the associated densification this corresponds to a ram speed of about 7 cm min^{-1}).

For comparison, conventionally cast aluminium and alloys of corresponding compositions (AlMg: 3.2, 5.8, 11.2 and 17.0 at % Mg; AlSi: 1.0, 2.3, 4.4, 8.0, 10.9, 14.4 and 19.0 at % Si) were extruded under identical conditions. For further details (melt-spinning equipment, precompaction and canning) see van Rooyen *et al.* [5].

2.2. Microscopy

Light microscopy (phase and interference contrast, conical illumination and bright field) was performed on longitudinal sections of the ribbons and on both longitudinal and transverse sections of the extrudates, using a Neophot-2 microscope (Carl Zeiss, Jena). Depending on the type of alloy the specimens were etched with Keller and Wilcox's reagent or electrolytically polished (Bath D2, Struers).

Scanning electron microscopy was applied using a JEOL JXA 50A instrument.

Transmission electron microscopy was performed with a Philips EM400 apparatus. Thin electron-transparent regions of the ribbons were investigated. Samples taken from the extruded bars were jet-electropolished (in a bath of 20% perchloric acid and 80% ethanol) before examination in the microscope.

2.3. X-ray diffraction

Lattice parameter determinations were performed using the Debye–Scherrer technique. For details see Mittemeijer *et al.* [8].

2.4. Hardness measurements

Hardness measurements were performed according to DIN 50133 applying a Leitz Durimet micro-Vickers hardness tester. The hardness measurements were carried out on longitudinal sections. To obtain reliable hardness values the distance between the centre of the indentation and the nearest edge of the specimen should be at least 2.5 times the average length of the diagonals of the diamond indentation. Therefore, when testing sections of the thin ribbons, a load of only 10 g was applied. Consolidates of aluminium, AlMg and AlSi alloys were tested on longitudinal sections of the extruded bars using loads of 50 and 25 g respectively.

2.5. Tensile testing

After removal by machining of the canning material from the extruded bars, specimens were prepared for tensile testing. The (longitudinal) tensile specimens were prepared according to DIN 50125 with a length/diameter ratio of 10. At least four specimens of each alloy were tested on an Instron tensile-testing machine (Model TTCML MI 1.4.6.).

3. Results and discussion

In a preceding paper [5] attention was paid to the extrusion process itself, including a (geometric) description of the bonding, stretching and alignment of the

TABLE I Alloying-element (silicon) content of liquid-quenched AlSi alloys. Gross content determined by chemical analysis; dissolved content determined by lattice-parameter measurements

Gross content (at %)	In solid solution (at %)
1.1	0.9
2.4	1.2
4.6	1.2
7.2	2.0
11.4	2.7
20.2	2.3

ribbons. Further, the benefits of an (in practice costly) degassing procedure (see Introduction) were examined. It was found that, under the present conditions, the preheating procedure applied was sufficient to obtain a sound product. An additional degassing in fact led to deterioration of the mechanical properties [5]. Therefore, in this paper results are reported only on undegassed materials.

3.1. Composition of ribbons and extrudates

The melt-spun AlMg ribbons were single-phase: all magnesium was in solid solution. However, the melt-spun AlSi ribbons were dual-phase (see Table I for the amount of silicon dissolved in the aluminium matrix). From a theoretical point of view it can be expected that the critical cooling rate above which the alloy solidifies as a single phase is higher for AlSi than for AlMg [9].

In the extruded AlMg alloys (both melt-spun and conventionally cast) with about 3 and 5 at % Mg, no trace of a second phase could be found. Optical micrographs of extrudates of AlMg alloys with about 11 at % Mg clearly showed small precipitates at grain boundaries (e.g. Figs 9c and 11c below). These grain-boundary precipitates are thought to develop during cooling of the extruded bars. In all extrudates of the 16.5 at % Mg alloy a homogeneous precipitation was observed by optical microscopy (see Fig. 9d below). X-ray diffraction demonstrated the presence of the β phase (about Al_8Mg_5). According to the phase diagram and the extrusion temperature applied for this alloy, the β phase already starts to precipitate during extrusion.

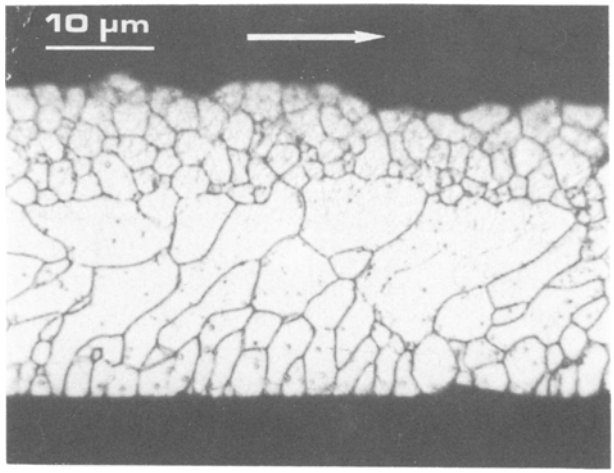

Figure 2 Longitudinal section of an AlMg (11.2 at % Mg) ribbon (etched with Keller and Wilcox's reagent; optical micrograph: bright field). Arrow indicates spinning direction.

The aluminium-rich matrix of the AlSi extrudates of both melt-spun and conventionally cast materials contained a small amount of dissolved silicon (about 0.5 at %). Apparently, at the extrusion temperature, precipitation had occurred until the equilibrium solubility was reached.

3.2. Morphology of the melt-spun ribbons

Typical examples are shown in Figs 1 to 4. In general, three zones can be discerned in the ribbons:

(i) Chill zone. Obviously, the highest cooling and solidification rates occur at the wheel side. This leads to very small crystallites in this region (showing sometimes an even "featureless" light-microscopical appearance) and the largest amount of dissolved alloying element (e.g. [10, 11]). Also, the structural imperfection as determined by X-ray diffraction line-broadening analysis is largest in the chill zone [12]. Further, the nearby presence of the heat sink induces a local thermal gradient perpendicular to the wheel surface, and this serves to explain an initial development of grain boundaries in the direction of the wheel-surface normal (Fig. 2).

(ii) Columnar grain zone. The unidirectional heat

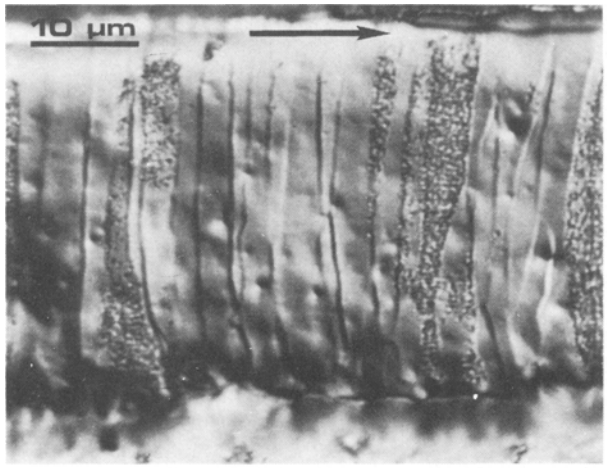

Figure 1 Longitudinal section of a pure aluminium ribbon (electrolyticaly polished; optical micrograph with interference contrast). Arrow indicates spinning direction.

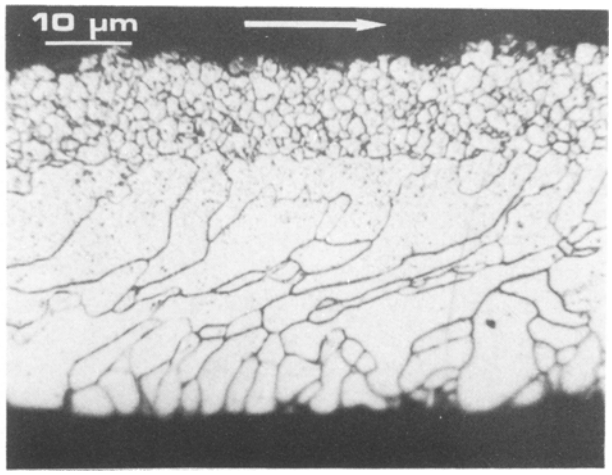

Figure 3 Longitudinal section of an AlMg (16.5 at % Mg) ribbon (etched with Keller and Wilcox's reagent; optical micrograph: bright field). Arrow indicates spinning direction.

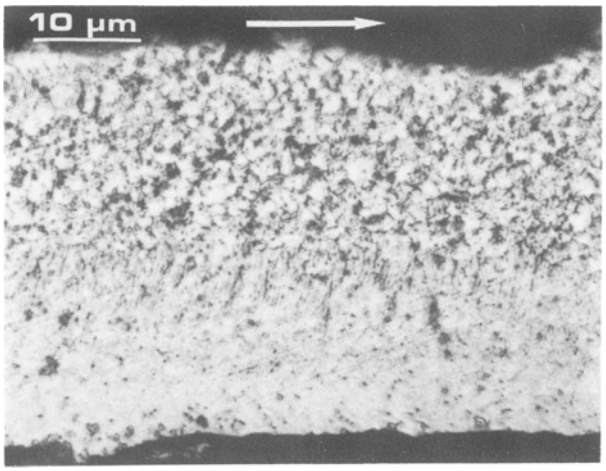

Figure 4 Longitudinal section of an AlSi (7.2 at % Si) ribbon (etched with Keller and Wilcox's reagent; optical micrograph: conical illumination). Arrow indicates spinning direction. Note zone of ultrafine columns in central region of the section.

flow condition in the puddle leads to columnar grains. It has been shown [13, 14] that with respect to the spinning direction, the thermal gradient in the puddle has an inclination in the reverse direction whereas near the solid–liquid interface the gradient of constitutional undercooling has a forward inclination. This could explain the occurrence of columns inclined forward with respect to the spinning direction. This is supported by Figs 1 to 3: in the case of (almost pure) aluminium there is (almost) no constitutional undercooling and therefore (almost) no column inclination, whereas for the AlMg ribbons the inclination increases with increasing magnesium content (i.e. increasing width of the solidus–liquidus gap). This columnar zone is also present in the AlSi ribbons, but can hardly be recognized because of the ultrafine grains (Fig. 4).

(iii) Equiaxed grain zone. The presence of equiaxed crystallites in the top layer is ascribed to a relatively slow heat transfer. This leads to nucleation in the liquid. In combination with convection in the liquid, equiaxed grains develop which are randomly oriented. Consistent with this conception, Fig. 5 shows that a slow heat transfer (because of an air bubble between the ribbon and the cooling wheel) indeed leads to a relatively thick layer of equiaxed crystallites.

Constitutional undercooling will also play an important role in the formation of the top layer of equiaxed crystallites [10]. Within this context Fig. 1 serves as an additional indication: in pure aluminium no constitutional undercooling occurs, and no top layer of equiaxed grains is observed.

The solidification history of melt-spun ribbons, showing the three-zone morphology, implies that segregation of alloying elements occurs in particular in the central region. This was demonstrated recently [10].

The increased fineness of microstructure, the increase of the amount of randomly oriented crystallites and the decrease of distinctness of preferred orientation with increasing alloying element content can be due to the hindrance of preferred growth by micro-segregation (AlMg) and/or second-phase particles (AlSi), both at grain boundaries.

The microstructure of the AlSi ribbons is much finer than that of the AlMg ribbons (cf. Figs 2 and 4): the second-phase silicon particles are very effective structure refiners (see also Fig. 6).

3.3. Morphology of the extrudates

3.3.1. Aluminium

Optical and transmission electron micrographs of extruded pure aluminium ribbons are shown in Figs 7a and b, respectively. Under the present conditions of extruding aluminium ribbons, the oxide layer, originally present on the ribbon surfaces, remains more or less intact (Figs 7a and b). The slightly fragmented oxide layer hinders intimate contact between the metallic bodies of the ribbons during extrusion. As a result, grain-boundary migration rarely occurred across the ribbon interfaces. In later stages of grain growth the grain boundaries within the ribbons extended from ribbon interface to ribbon interface and advanced in lateral directions (Fig. 7a).

As indicated by the oxide layers at the ribbon interfaces, during extrusion the ribbons are stretched and aligned roughly parallel to the extrusion direction (Fig. 7a, see also van Rooyen *et al.* [5]).

The oxide-layer barrier to grain growth is obviously absent for the conventionally cast aluminium, and hence very large crystals develop (Fig. 8; note the difference in magnification between Figs 7a and 8). It can reasonably be expected that on hot extrusion of both melt-spun and conventionally cast aluminium dynamic recovery occurs [15], and thus the observed recrystallization/grain growth was dominant during cooling after extrusion.

3.3.2. Aluminium–magnesium

Micrographs of extruded AlMg ribbons are shown in Figs 9a to d. As compared to extruded ribbons of pure aluminium, AlMg has thicker oxide layers at the ribbon interfaces: electron microprobe analyses showed that at these locations a large amount of oxygen is present and that the Mg/Al ratio is significantly larger

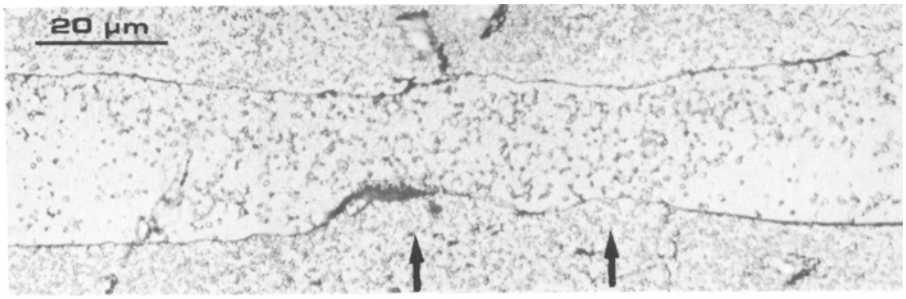

Figure 5 Longitudinal section of an AlMg (16.5 at % Mg) ribbon (electrolytically polished; optical micrograph: bright field). At the location where an air bubble was enclosed (arrow) between ribbon and wheel, the chill zone is absent.

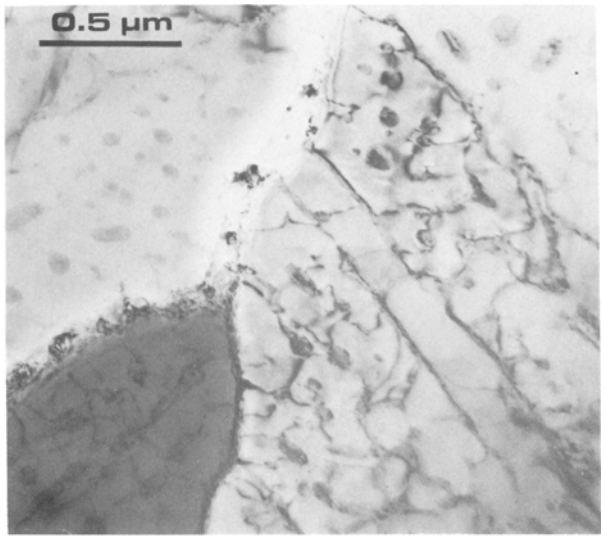

Figure 6 Transmission electron micrograph (bright field) of an AlSi (4.6 at % Si) ribbon, viewed in the direction of the surface normal. Note the small silicon particles.

than in the bulk. (In view of the oxide layer thickness and the microprobe spot size only semi-quantitative analyses were possible.) The latter observation agrees with results obtained in an investigation of the oxidation of conventionally cast aluminum alloys [16]. It can be concluded that during extrusion of AlMg ribbons no sufficient fragmentation of oxide layers occurred to establish a predominantly metallic contact between the ribbons.

In particular, for magnesium contents larger than about 3 at % dynamic recrystallization occurred during extrusion (a further discussion is given in Section 3.4.1.2.). The grain growth was generally restricted to within the (former) ribbon surfaces, as a consequence of the presence of the oxide layers. Grain growth is retarded by the solute-drag effect: the larger the amount of magnesium atoms dissolved, the smaller the final grain size (Figs 9a to d). This distinct effect is also clearly apparent in the microstructures of the extruded conventionally cast alloys (Figs 10a to d). In the latter case the grain growth is obviously not impeded by oxide layers.

The development of numerous second-phase particles during extrusion of the AlMg (16.5 at % Mg) alloy (see Section 3.1) provides an additional grain-growth impeding factor as evidenced by a comparison of grain-size differences between Figs 10a to c and Fig. 10d.

In contrast with the aluminium ribbons, the AlMg ribbons exhibit after extrusion more X-ray diffraction line-broadening (Debye–Scherrer phtographs) than before. This corresponds with the presence of many deformation-induced dislocations (cf. Fig. 11 and Fig. 7b). The dissolved magnesium atoms form effective obstacles to dislocation movement.

3.3.3. Aluminium–silicon

Micrographs of extruded AlSi ribbons are shown in Figs 12a to d. As in the case of the ribbons, all extrudates are dual-phase: silicon particles at grain boundaries and within grains of the aluminium matrix are clearly visible (see also Fig. 13). With reference to the melt-spun ribbons, the size of the silicon particles in the extrudates is much larger (cf. Figs 6 and 13). Ribbon interfaces are only slightly visible after etching, implying that, as compared with the AlMg alloys, a much more intimate contact between the ribbons was established by extrusion. (In this connection it can be remarked that oxidation of AlMg leads to porous, thick oxide layers, whereas oxidation of AlSi results in seclusive, thin oxide layers [16].) Furthermore, the grain size of the AlSi consolidates decreases with increasing silicon content and is much smaller than that of the AlMg consolidates. This result can be ascribed to grain-boundary pinning by second-phase particles during extrusion, whereas the AlMg alloys were single-phase during extrusion (except the AlMg (16.5 at % Mg) alloy).

Obviously, the matrix grain sizes and the second-phase particles are much larger for the extruded conventionally cast than for the extruded liquid-quenched AlSi alloys (Figs 14a to d). In the conventionally cast

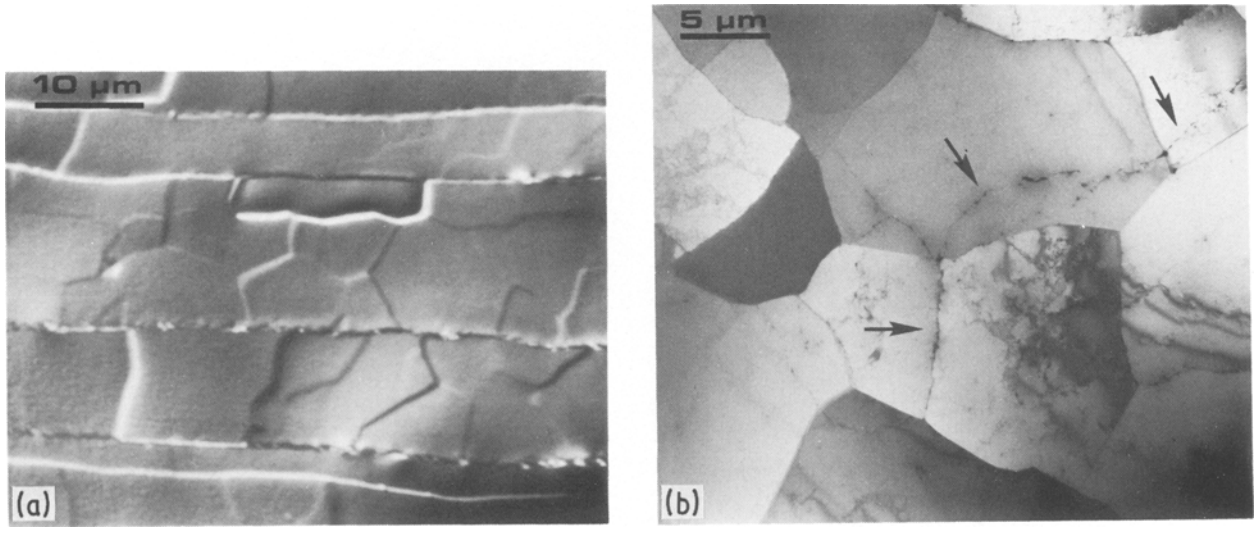

Figure 7 (a) Longitudinal section of consolidate of pure aluminium ribbons (electrolytically polished; optical micrograph: interference contrast). (b) Transmission electron micrograph (bright field) of consolidate of pure aluminium ribbons. Arrows indicate oxide layer.

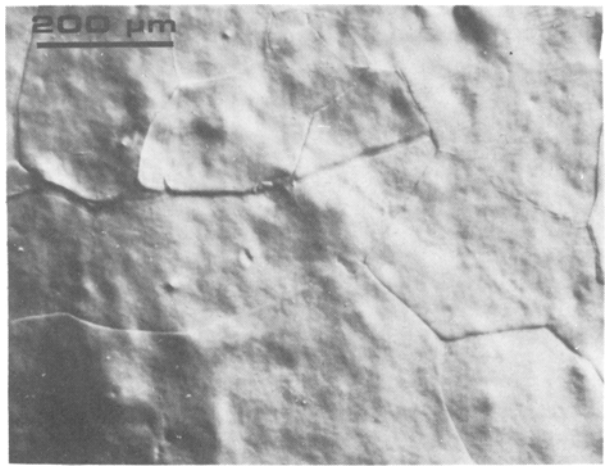

Figure 8 Longitudinal section of extruded conventionally cast pure aluminium (electrolytically polished; optical micrograph: interference contrast).

AlSi (20.2 at % Si) alloy, very large faceted primary silicon particles are present (Fig. 14d). During the deformation process the interaction between these relatively hard and brittle particles and the relatively soft and ductile matrix can lead to porosity at the interfaces, as can be seen in Figs 14d and 15.

3.4. Mechanical properties

3.4.1. Aluminium–magnesium

3.4.1.1. Hardness. The hardness of the melt-spun AlMg ribbons as a function of magnesium content is presented in Fig. 16. All magnesium is in solid solution after liquid quenching (Section 3.1). Hence, the increase of hardness with increasing magnesium content can be ascribed to solid-solution strengthening. Guinier–Preston (GP) zone formation during ageing at room temperature can contribute to the enhanced hardness increase observed for the AlMg (16.5 at % Mg) alloy. This GP-zone formation occurs significantly for magnesium contents larger than about 10 at % [17].

The increase of the flow stress, $\Delta\tau$, due to misfitting solute atoms, can be represented [18] by

$$\Delta\tau = \tfrac{1}{4}\mu\varepsilon C^{1/2}$$

where μ = shear modulus, ε = linear misfit parameter and C = solute atom concentration. The hardness is proportional to the flow stress [19]. Then, in the case of solid-solution hardening, a linear relation would occur between hardness increase and the square root of solute atom concentration. This is indeed observed for the AlMg ribbons, where no significant GP-zone formation occurred (Fig. 17). The deviation observed for the AlMg (16.5 at % Mg) alloy can be due to the presence of GP zones (see above discussion).

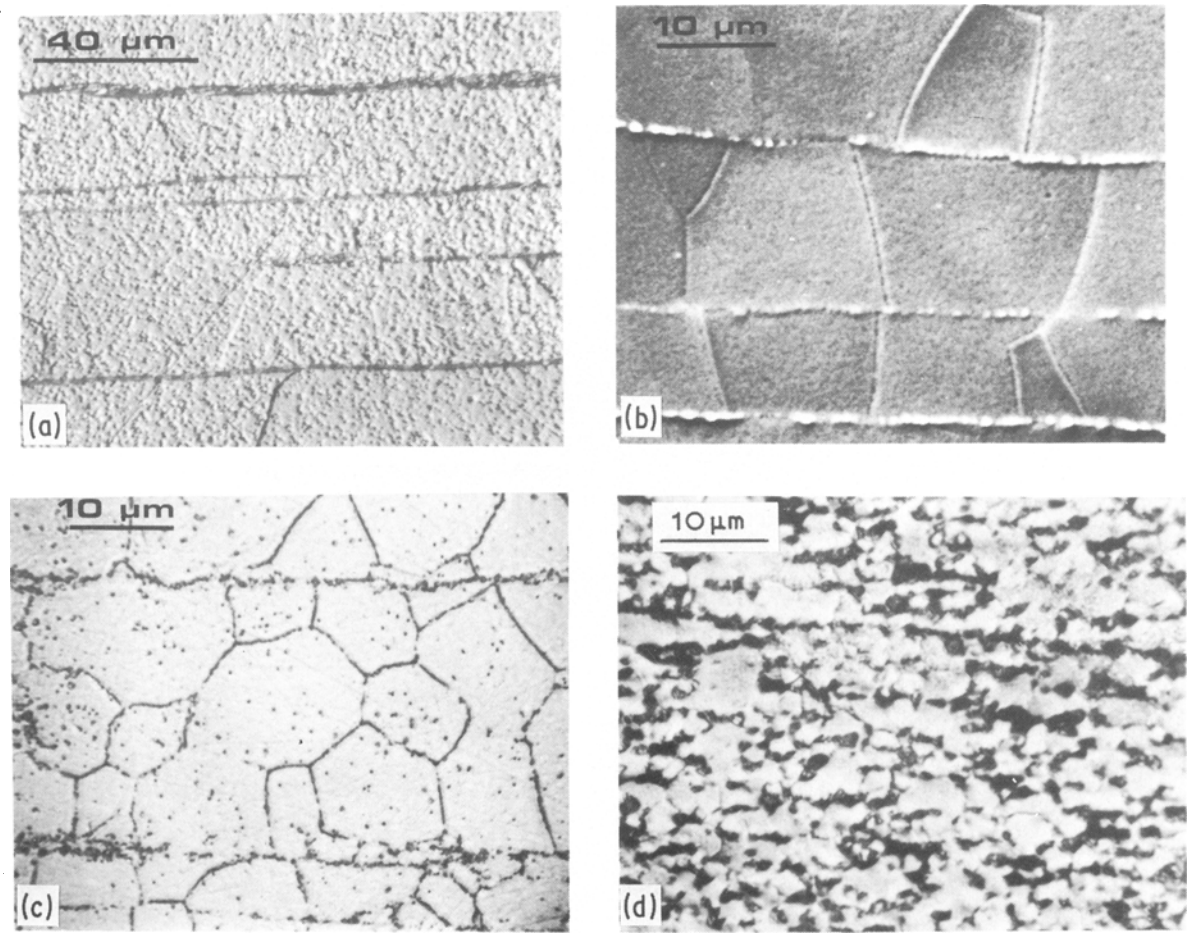

Figure 9 Longitudinal sections of consolidates of AlMg ribbons. (a) 2.6 at % Mg; etched with Keller and Wilcox's reagent; optical micrograph: interference contrast. (b) 5.6 at % Mg; electrolytically polished; scanning electron micrograph. (c) 11.2 at % Mg; etched with Keller and Wilcox's reagent; optical micrograph: conical illumination. (d) 16.5 at % Mg; electrolytically polished; optical micrograph: interference contrast.

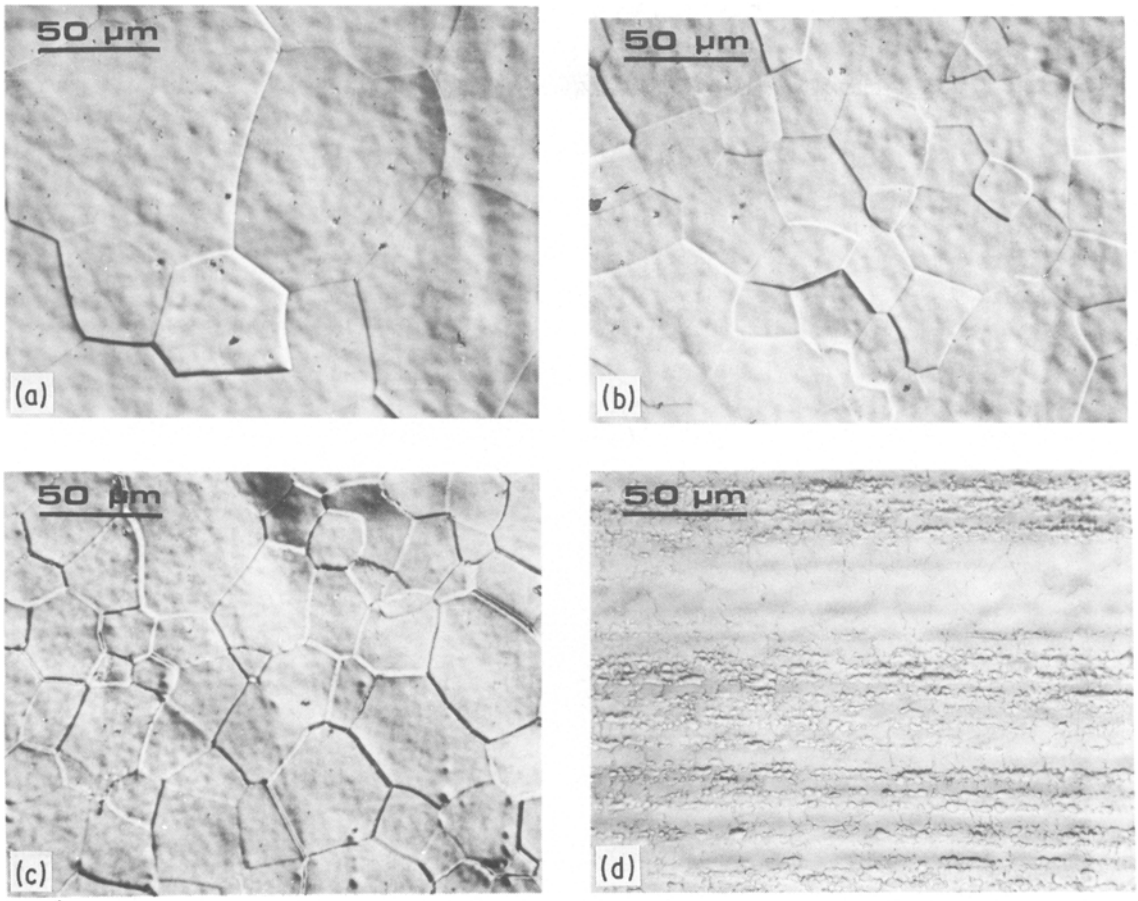

Figure 10 Longitudinal sections of extruded conventionally cast AlMg alloys. (a) 3.2 at % Mg; electrolytically polished; optical micrograph: interference contrast. (b) 5.8 at % Mg; electrolytically polished; optical micrograph: interference contrast. (c) 11.2 at % Mg; electrolytically polished; optical micrograph: interference contrast. (d) 17.0 at % Mg; electrolytically polished; optical micrograph: interference contrast.

The AlMg ribbon extrudates are dominantly single-phase, except for the AlMg (16.5 at % Mg) alloy (see Section 3.1). Thus solid-solution strengthening again explains the hardness increase observed on alloying (Fig. 16). However, as compared with the liquid-quenched state, the pronounced increase of grain size provoked by extrusion (cf. Figs 2 and 9c) leads to a general decrease of hardness (Fig. 16). This hardness decrease is most pronounced for the AlMg (16.5 at % Mg) alloy, which is attributed to the precipitation of (coarse) β particles in (only) this alloy during extrusion (cf. Figs 3 and 9d).

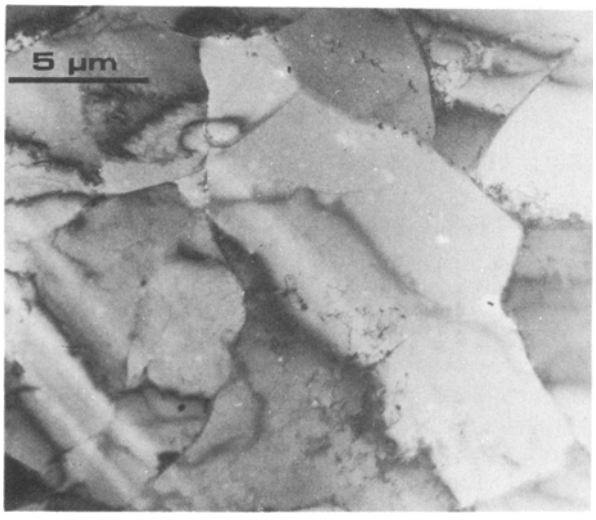

Figure 11 Transmission electron micrograph (bright field) of consolidate of AlMg (3.2 at % Mg) ribbons. Note contrast due to dislocations.

3.4.1.2. Tensile properties of extrudates. The ultimate tensile strength as a function of magnesium content is shown in Fig. 18. In accordance with the discussion in Sections 3.1 and 3.3 the initial increase in tensile strength is ascribed to solid-solution strengthening. At higher magnesium contents, precipitation of β particles at (former) ribbon/grain boundaries (Fig. 9d) affects the tensile strength. As discussed in Section 3.3.2, hardly any grain growth across the original ribbon surfaces had occurred, implying an insufficient bonding of the constituents in the consolidated product. As a consequence the tensile strength of the consolidated ribbons is not better (and in transverse directions even worse [5]) than that of the extruded conventional castings (Fig. 18).

The elongation at fracture is presented in Fig. 19 as a function of magnesium content. Initially, the elongation decreases with increasing magnesium content and a minimum occurs at about 3 at % Mg. For larger magnesium contents the elongation increases, reaches a plateau value, and eventually declines rapidly. This peculiar behaviour may be explained as follows. In pure aluminium, recovery processes occur during hot extrusion (dynamic recovery). This has been

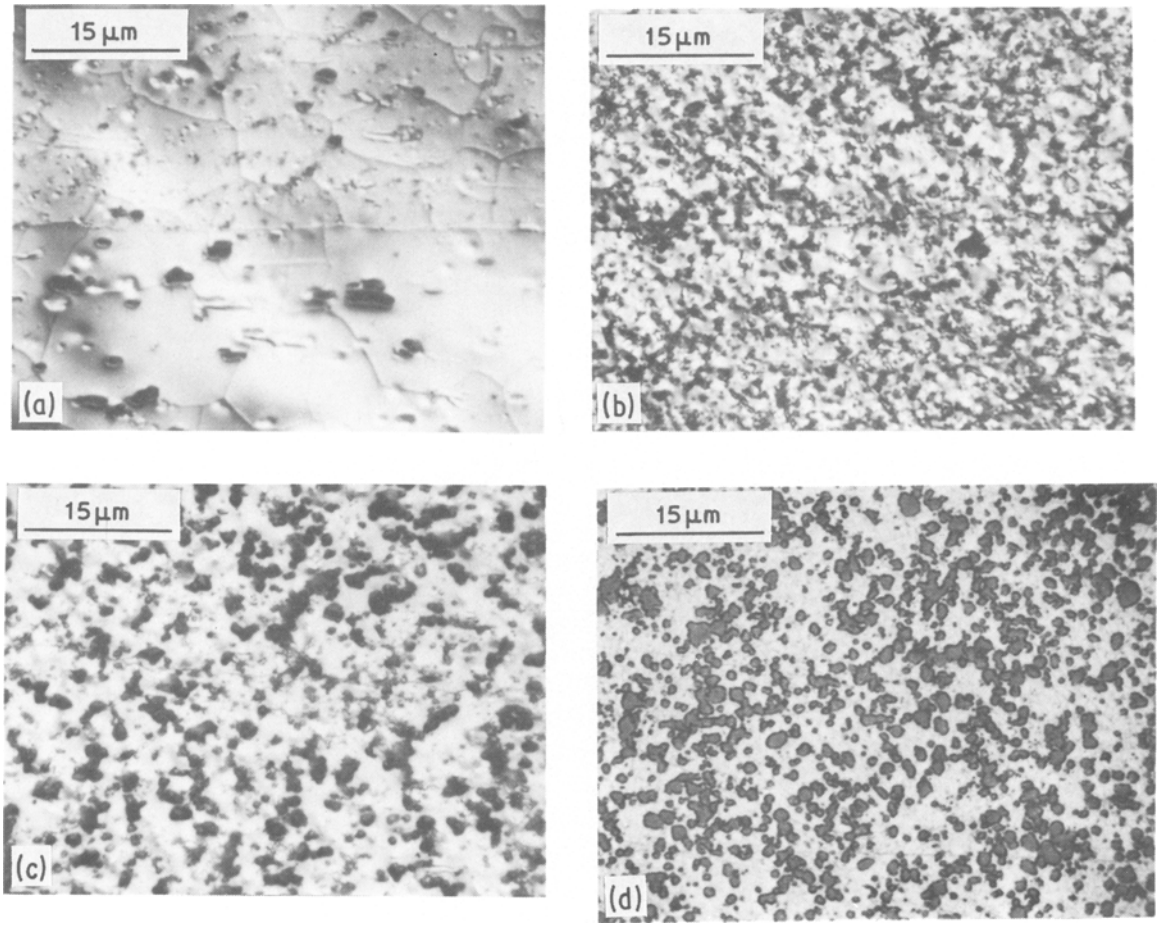

Figure 12 Longitudinal sections of consolidates of AlSi ribbons. (a) 1.1 at % Si; electrolytically polished and subsequently etched with Keller and Wilcox's reagent; optical micrograph: interference constrast. (b) 4.6 at % Si; electrolytically polished and subsequently etched with Keller and Wilcox's reagent; optical micrograph: interference contrast. (c) 11.4 at % Si; electrolytically polished and subsequently etched with Keller and Wilcox's reagent; optical micrograph: interference contrast. (d) 20.2 at % Si; unetched; optical micrograph: conical illumination.

ascribed to a high stacking-fault energy [15]. As a result a relatively high ductility is observed. Indications exist that alloying with magnesium lowers the stacking-fault energy [20] (but see discussion in Sheppard *et al.* [21]). It can then be anticipated that a less pronounced recovery occurs during extrusion (compare Figs 11 and 7b). Consequently, the ductility after hot extrusion continuously decreases with increasing magnesium content. Apparently the decrease of grain size on alloying with magnesium compensated only partly for this effect. Ultimately, on increasing the magnesium content, dynamic recrystallization is provoked which corresponds with an increase of the ductility. The appearance of β particles at ribbon/grain boundaries after extrusion at high magnesium contents is obviously accompanied by a low ductility.

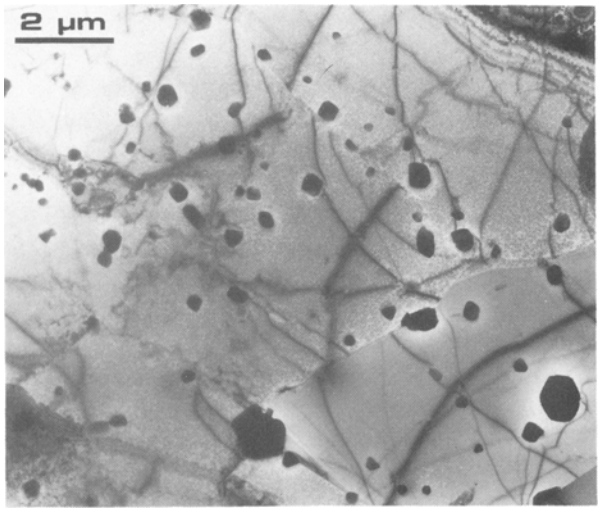

Figure 13 Transmission electron micrograph (bright field) of consolidate of AlSi (1.3 at % Si) ribbons.

3.4.2. Aluminium–silicon

3.4.2.1. Hardness. All AlSi ribbons are dual-phase after liquid quenching. The maximal amount of dissolved silicon occurs at about the eutectic composition (Table I and Bendijk *et al.* [11]). Both solid-solution and dispersion strengthening mechanisms explain the hardness increase observed on alloying with silicon, with a relatively important contribution of solid-solution strengthening for the lower silicon contents (Fig. 20).

For ribbon extrudates, the amount of silicon dissolved in the aluminium matrix is approximately equal to the maximal amount dissolved in equilibrium at the preheat temperature (equal to about 0.5 at % Si; see Section 3.1.). Consequently, as compared with the liquid-quenched state, the contribution of solid-solution strengthening to the observed hardening is much smaller. Further, a coarsening of the dual-phase

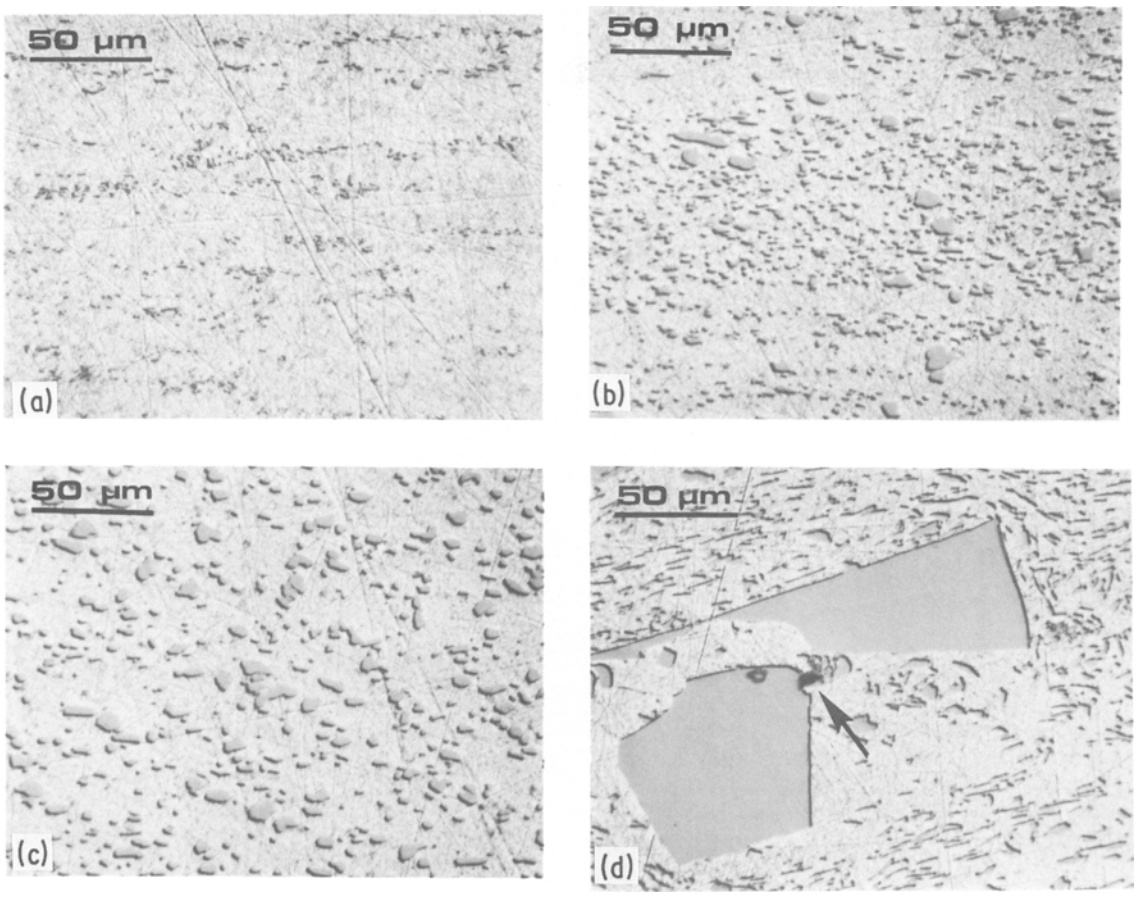

Figure 14 Longitudinal sections of extruded conventionally cast AlSi alloys. (a) 2.3 at % Si; etched with Keller and Wilcox's reagent; optical micrograph: interference contrast. (b) 8.0 at % Si; etched with Keller and Wilcox's reagent; optical micrograph: interference contrast. (c) 14.4 at % Si; etched with Keller and Wilcox's reagent; optical micrograph: interference contrast. (d) 19.0 at % Si; etched with Keller and Wilcox's reagent; optical micrograph: interference contrast. Arrow indicates void; see also Fig. 15.

microstructure is induced by extrusion (cf. Figs 6 and 12b). Both effects serve to explain the general decrease of hardness observed after extrusion (Fig. 20).

3.4.2.2. Tensile properties of extrudates. The ultimate tensile strength is shown in Fig. 21 as a function of silicon content. As discussed above for the dependence of hardness on silicon content, strengthening in the AlSi extrudates mainly stems from the dispersed silicon phase; only 0.5 at % Si is dissolved in the matrix after extrusion. In contrast with the AlMg extrudates, for the AlSi extrudates (in particular those with a high silicon content) the tensile strength of extruded ribbons is significantly larger (up to 50%) than that of extruded conventionally cast material. This difference between AlMg and AlSi extrudates originates (see Section 3.3.3.) from

(i) the moderate coarsening of the AlSi microstructure on extrusion, where the final microstructure of the AlSi extrudates is much finer for the ribbon material than for the conventionally cast material (cf. Figs 12d and 14d; note the difference of magnification); and

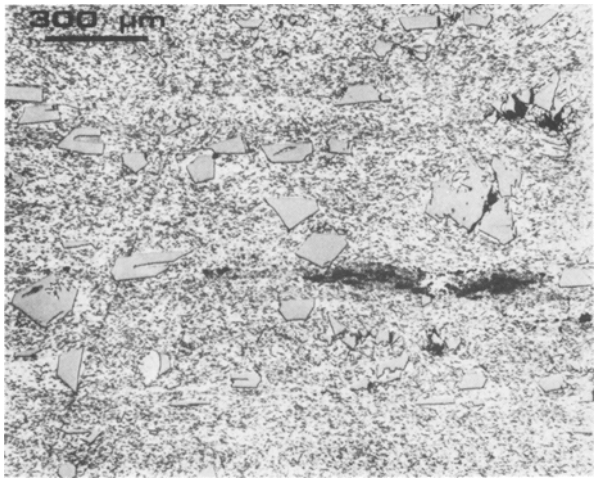

Figure 15 Longitudinal section of extruded conventionally cast AlSi (19.0 at % Si) alloy (etched with Keller and Wilcox's reagent; optical micrograph: interference contrast). Note the porosity.

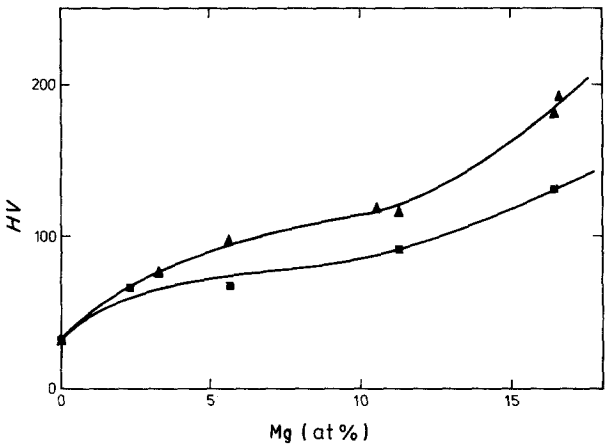

Figure 16 Microhardness of (▲) ribbons and (■) consolidates of AlMg as a function of gross magnesium content.

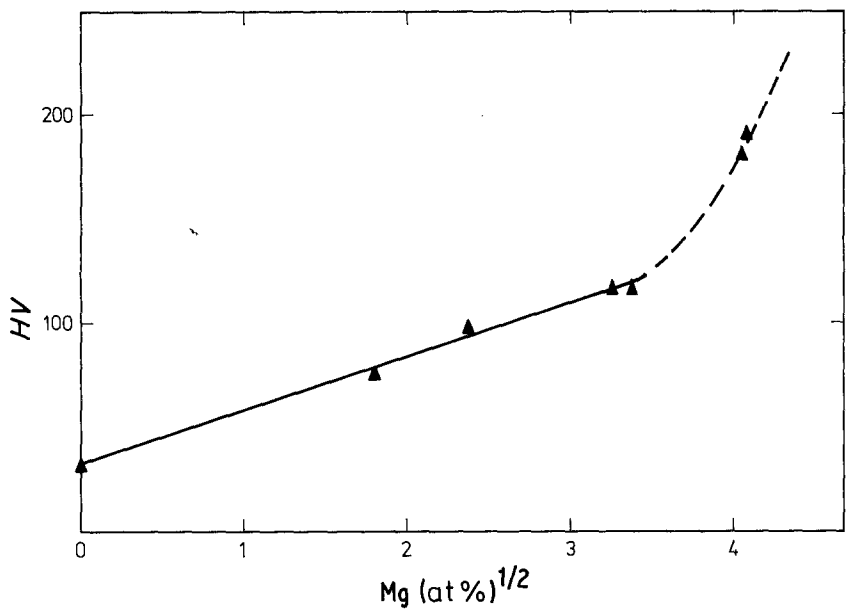

Figure 17 Microhardness of AlMg ribbons as a function of square root of gross magnesium content.

(ii) a strong bonding between the consolidated ribbons.

The elongation at fracture of the consolidated materials decreased on alloying with silicon. The elongations at about 20 at % Si were 12 and 4% for the extruded ribbons and the extruded conventionally cast materials, respectively. This difference, too, can be considered as a result of the relatively small grain size occurring in the consolidated ribbon material (see above).

4. Conclusions

4.1. Composition

1. In the as-liquid-quenched condition the AlMg alloys were single-phase, whereas the AlSi alloys were dual-phase.

2. After consolidation the composition of the aluminium-rich phase of the AlMg and AlSi ribbon material corresponded with the equilibrium solid solubility of the alloying element at the extrusion temperature.

3. Oxide layers at the ribbon surfaces were more pronounced for AlMg than for AlSi.

4.2. Morphology

1. As a combined result of heat-flow conditions and constitutional undercooling, in general the melt-spun alloys exhibited a three-zone morphology.

2. On extruding ribbon material, coarsening of the microstructure occurred with the growth of grains (AlMg and AlSi) and second-phase particles (AlSi). Grain growth was restricted mainly to within the original ribbon surfaces.

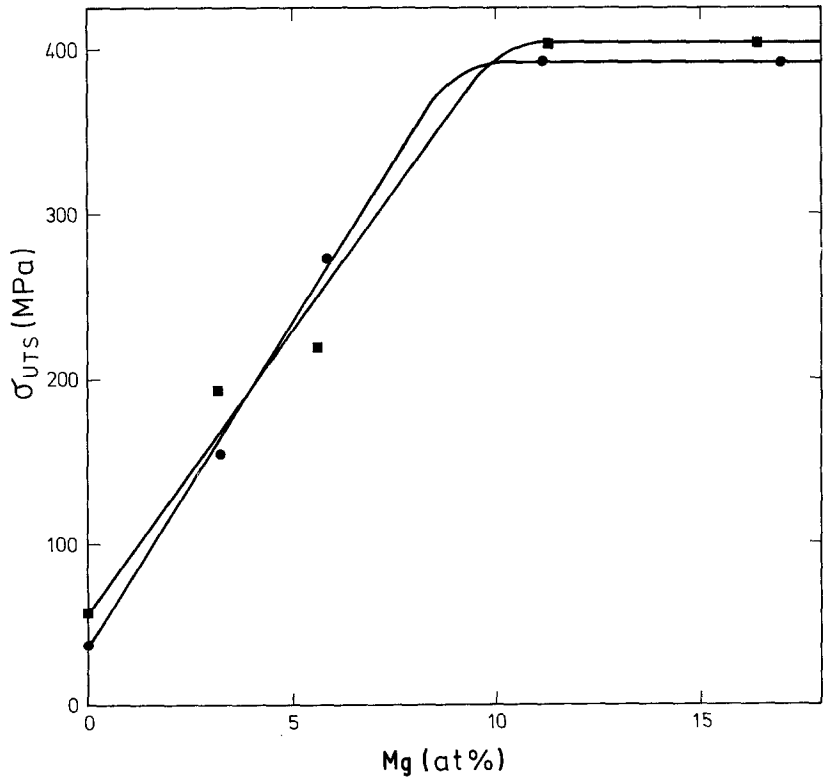

Figure 18 Ultimate tensile strength, σ_{UTS}, of (■) consolidated ribbons and (●) extruded conventional castings of AlMg as a function of gross magnesium content.

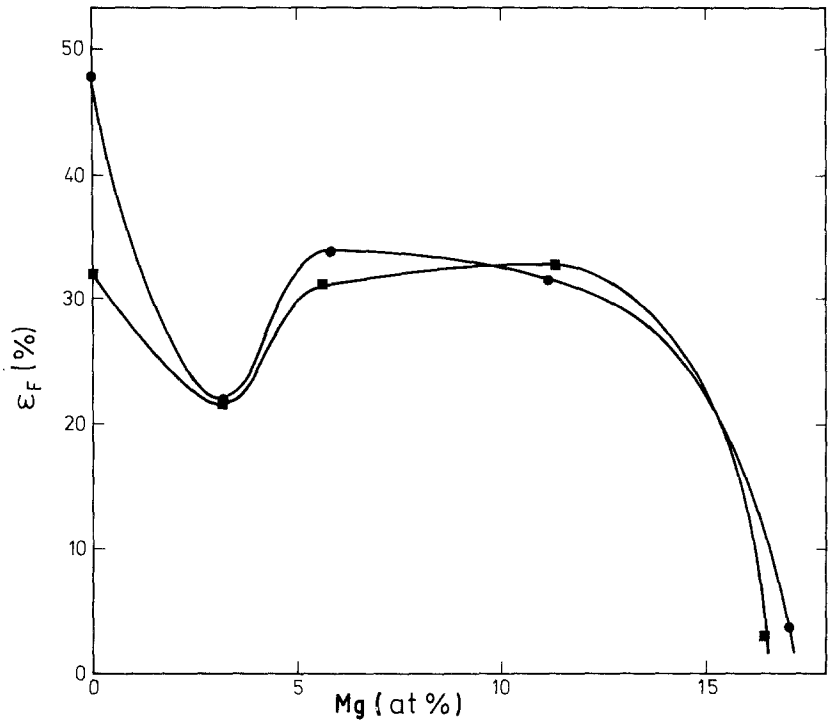

Figure 19 Elongation at fracture, ε_F, of (■) consolidated ribbons and (●) extruded conventional castings of AlMg as a function of gross magnesium content.

3. The microstructure became finer with increasing alloying-element content. This can be ascribed to solute-drag effects (in particular for AlMg) and the pinning of grain boundaries by second-phase particles (in particular for AlSi).

4. Second-phase particles as in AlSi are very effective structure refiners.

5. The microstructure of extruded ribbon material was much finer than that of extruded conventionally cast material of corresponding composition.

4.3. Hardness

1. The hardness of the AlMg ribbon material increased with increasing magnesium content as a result of solid-solution strengthening, implying a linear relation between the hardness and the square root of solute-atom concentration. The extrusion-induced increase of grain size contributed to a significant decrease in hardness.

2. The hardness of the AlSi ribbon material increased with silicon content as a result of both dispersion strengthening and solid-solution strengthening. The extrusion-induced increase of grain size and the progress of precipitation/coarsening of the second phase contributed to a drastic decrease in hardness.

4.4. Tensile properties

1. The increase of the tensile strength of consolidated AlMg and AlSi ribbon material with increasing alloying-element content is predominantly caused by solid-solution and dispersion strengthening respectively.

2. Relatively thick oxide layers (as with AlMg) hinder an intimate metallic contact between ribbons on extruding, which affects the tensile strength.

3. The decrease and subsequent increase of the elongation at fracture on increasing the alloying-element content in extruded AlMg alloys is ascribed to

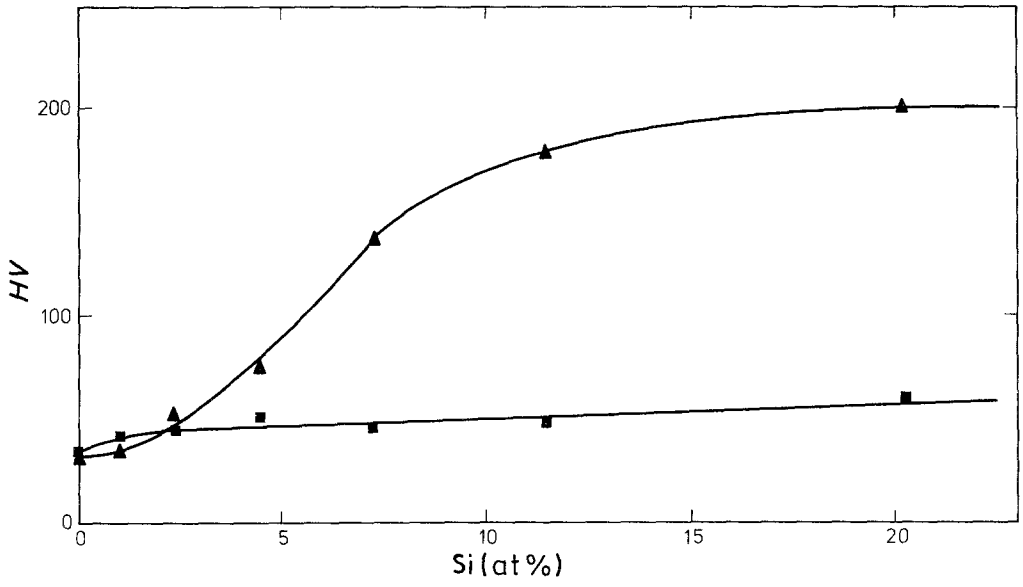

Figure 20 Microhardness of (▲) ribbons and (■) consolidates of AlSi as a function of gross silicon content.

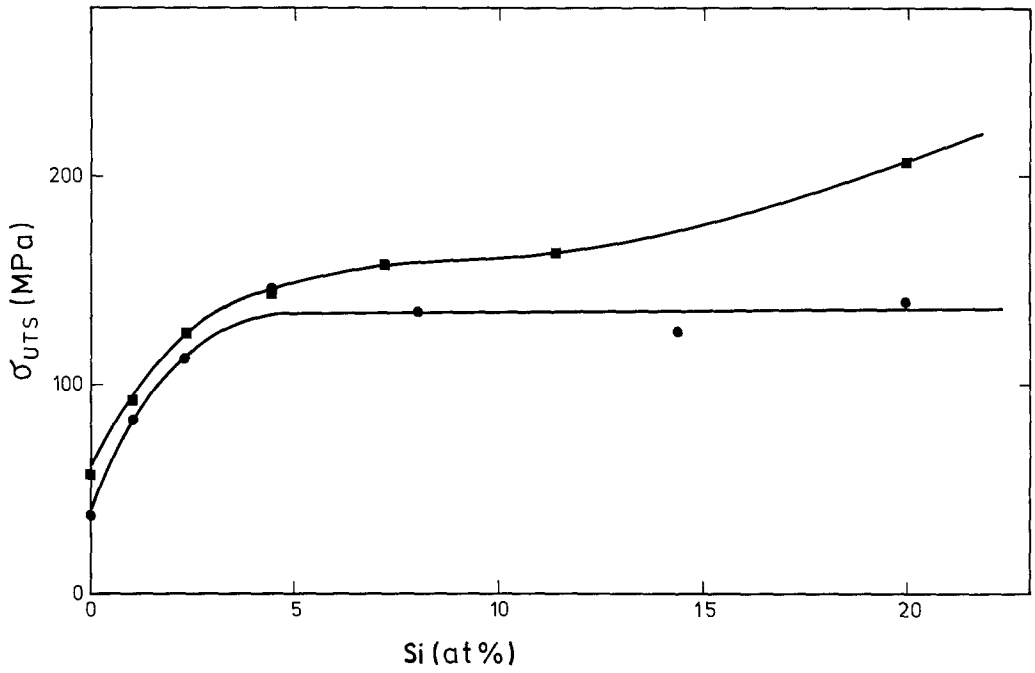

Figure 21 Ultimate tensile strength, σ_{UTS}, of (■) consolidated ribbons and (●) extruded conventional castings of AlSi as a function of gross silicon content.

the predominance of either dynamic recovery (below about 3 at % Mg) or dynamic recrystallization (above about 3 at % Mg).

4. In contrast to the extruded AlMg ribbon material, the tensile strength of extruded AlSi ribbon material was significantly larger than that of extruded conventionally cast material of corresponding composition. This difference was most pronounced at higher amounts of alloying element (tensile-strength improvement of 50% at about 20 at % Si).

Acknowledgements

The authors are indebted to Professor B. M. Korevaar for stimulating discussions. Ir. P. van Mourik performed the X-ray diffraction lattice parameter determinations, Mr C. D. de Haan carried out the transmission electron microscopy and Mr D. P. Nelemans did the scanning electron microscopy and electron-microprobe analysis. Financial support by the Foundation for Fundamental Research of Matter (FOM) is gratefully acknowledged.

References

1. R. W. CAHN, *Int. J. Rap. Sol.* **1** (1984) 81.
2. G. E. DIETER, "Mechanical Metallurgy" (McGraw-Hill, London, 1976) Ch. 5.
3. H. JONES, *J. Mater. Sci.* **19** (1984) 1043.
4. R. E. MARINGER, *SAMPE Q.* **12** (1980) 30.
5. M. VAN ROOYEN, J. A. VAN DER HOEVEN, L. KATGERMAN, P. VAN MOURIK, TH. H. DE KEIJSER and E. J. MITTEMEIJER, in Proceedings of the P.M. Aerospace Materials Conference, Berne (Switzerland), November 1984, Vol. 1, edited by Metal Powder Report, p. 341.
6. T. SHEPPARD, *Met. Technol.* **8** (1981) 130.
7. Proceedings of P.M. Aerospace Materials Conference, Berne (Switzerland), November 1984, Vols. 1 and 2, edited by Metal Powder Report.
8. E. J. MITTEMEIJER, P. VAN MOURIK and TH. H. DE KEIJSER, *Phil. Mag.* **43A** (1981) 1157.
9. L. KATGERMAN, *Scripta Metall.* **17** (1983) 537.
10. J. A. VAN DER HOEVEN, P. VAN MOURIK and E. J. MITTEMEIJER, *J. Mater. Sci. Lett.* **2** (1983) 158.
11. A. BENDIJK, R. DELHEZ, L. KATGERMAN, TH. H. DE KEIJSER, E. J. MITTEMEIJER and N. M. VAN DER PERS, *J. Mater. Sci.* **15** (1980) 2803.
12. R. DELHEZ, TH. H. DE KEIJSER, E. J. MITTEMEIJER, P. VAN MOURIK, N. M. VAN DER PERS, L. KATGERMAN and W. E. ZALM, *ibid.* **17** (1982) 2887.
13. K. TAKESHITA and P. H. SHINGU, *Trans. Jpn. Inst. Met.* **24** (1983) 529.
14. L. KATGERMAN, in Proceedings of 5th International Conference Rapidly Quenched Metals, Würzburg, September 1984, p. 819.
15. H. J. McQUEEN, *J. Metals* **32** (1980) 2.
16. H. J. VAN BEEK, MSc thesis, Delft University of Technology (1984).
17. J. A. SINTE MAARTENSDIJK, MSc thesis, Delft University of Technology (1985).
18. P. M. KELLY, *J. Aust. Inst. Metals* **16** (1971) 104.
19. J. R. CAHOON, W. H. BROUGHTON and A. R. KUTZAK, *Metall. Trans.* **2** (1971) 1979.
20. H. M. TENSI, P. DROPMAN and H. BORCHERS, *Z. Metallkde* **61** (1970) 518.
21. T. SHEPPARD, N. C. PARSON and M. A. ZAIDI, *Met. Sci.* **17** (1983) 481.

Received 19 July
and accepted 16 September 1985